Hybrid Inorganic-Organic Cyclophosphazene-Phenothiazine Based Material with Tunable Yellow-Green Emitting Properties

Dinesh Kumar Chelike[1,2*],

[1]Department of Chemistry, Rungta College of Engineering & Technology, Bhilai-490024 Chhattisgarh, India

Senthil A. Gurusamy Thangavelu[2] and Ananthanarayanan Krishnamoorthy[2]

[2]Research Institute, Department of Chemistry, SRM Institute of Science & Technology, Kattankulathur, Chennai-603203 Tamil Nadu, India

Abstract

Cyclophosphazene hydrazide (CTP-Hyd) and six components of R-PTZ-CHO were condensed to generate a unique luminous hybrid inorganic-organic molecule structure. For the first time, the phenothiazine (PTZ) unit have been appended to the edge of the thermally stable CTP core ring through condensation using the new precursor synthesised from an inorganic heterocycle, CTP-Hyd. ATR-FTIR, ^{1}H-NMR and ^{13}C-NMR used to illustrate the luminous hybrid material. Additionally, UV-vis spectroscopy, photoluminescence spectroscopy, cyclic voltammeter (CV) and Thermo gravimetric analysis (TGA) were utilised to examine the photophysical and thermal properties of the hybrid material. In the chapter, we have solely addressed the characterisation of the hybrid material, as well as its photophysical and electrochemical properties.

Keywords: Cyclophosphazene, phenothiazine, hybrid material, photophysical properties, inorganic-organic hybrid compound.

I INTRODUCTION

In order to investigate diverse application, including those in the fields of photophysics and photochemistry, hybrid inorganic-organic framework has recently been produced employing the association of several chromophore units on an inorganic structure [1-5]. Advantages of organic units in terms of stability, thermal, mechanical and physiochemical features found to improve in these hybrid systems [6-8]. The choice of prospective synthons and an effective method must be devised in order to support the reciprocal involvement of organic-inorganic compounds in hybrid structures [9,10]. In earlier studies [5,11-14], such rhodamin, phthalocyanine, fluorescein, fluorine, anthracene, naphthol, dansyl, phenanthroline, pyrene and bianthracence were investigated as an organic analogue of hybrid assembly. Phenothiazine (PTZ), among other organic molecules, was chosen for this study due to it's special ability to have bowl shaped non-planar hetero-aromatic assembly accompanied via nitrogen and sulphur atoms with a tendency to prolong conjugation. The synthesis of donor-acceptor features in the texture of pristine PTZ can be achieved by simple chemical method, such as formylation and N-alkylation, resulting in R-PTZ-CHO (R = $-C_7H_{18}$) [15]. R-PTZ-CHO was endangered to condense with tris-(2-aminoethyl)amine to formulate Schiff's base and their photo physical character was studied [16,17]. In fact, when incorporating on support of an inorganic units, the desirable features of such organic moiety frequently tent to be proficiently utilised [12,18]. Cyclophosphazene, CTP, an inorganic heterocycle was well known for its planar ring structure and stiff cyclic skeleton, $[-N=PCl_2]_3$ with six reactive chlorines and its ability to undergo nucleophile substitution with various organic reagents (-OH, $-NH_2$, -SH etc.) [19-21].

In the previous works we establish to noticed a few examples of hybrid assemblies based on the interaction of organic moiety tethered with amine/hydroxyl group via inorganic heterocycles [5,11-14]. These hybrid products displayed distinctive photophysical and electrochemical feature. In order to enhance the reactive nature of hydroxyl group substances, CTP was added via an aryloxy linkage to a variety of organic compound, including oxy-naphthylchacone, porphyrin, fulleropyrrolidine-pyridine, hexaboron-dipyrromethene, adamantine and imidazole/benzimidazole [22-27]. The amine group of organic compound such as phenanthroline, naphthalene and 9-aminophenalenimine was also used to produce a reaction with CTP [28-31]. These studies promote us to produce

a newly kind of CTP-Hyd as an inorganic counterpart to obtain a unique gathering of six PTZ components through condensation reaction with R-PTZ-CHO (R = -C_8H_{17}) to generate hexakis hydrazine Schiff's base of PTZ on periphery of CTP for the first time in our previous report [32]. Before demonstrating the recently established CTP-Hyd such as a key support in the current study, the significant studies on the chemistry of phosphorus (P) hydrazide and it's analysis must be discussed. For the resolve of generating P(V) hydrazides, which are easily converted into hydrazone Schiff's bases moiety of macrocycles, dendtrimers and multi-site ligands for a variety of application [12,32-36]. Such P(V) hydrazide found to Synthesised with terminal amine group (-NH_2) subsequently regiospecific substitution at the core of –NH(Me). Despite the hydrazone established from CTP-Hyd would be separate because the primary amine group (-NH_2) that is next to the secondary (-NH-) amine replaced at the P(V) centre implicated in the synthesis of Schiff's base and hydrazone bonds among inorganic and organic moieties. In this chapter, CTP-PTZ is a unique example, Synthesised as an assembly of six PTZ moieties on CTP ring through simple condensation between the CTP-Hyd and R-PTZ-CHO under feasible reaction condition.

II METHODOLOGY

The convergent method, as shown in **scheme 1**, was used to synthesise the CTP-PTZ hybrid substrate. The tough and reactive inorganic core of CTP structure, which has six chlorine atoms was preferred to utilised the array of organic subtract due to the reactive nature, six units of PTZ structure at the periphery of three P(V) centres in the absence of steric hindrance [39]. In order to establish an electron withdrawing formyl group (-CHO) at the 3rd position of an aromatic ring structure (PTZ), $POCl_3$ was added to N,N'-dimethylformamide (DMF) in an ice cold condition, followed by a reaction with octyl substituted with PTZ in dichloroethane medium under reflux circumstances [15]. In another aspect, after the removal of hydrazine hydrochloride (NH_2-NH_2.HCl) at room temperature, cyclophosphazene hydrazide (CTP-Hyd) was produced by rapidly substituting all chlorine atoms through a nucleophile substitution process utilising excessive hydrazine hydrate in chloroform medium. In the synthesis of CTP-PTZ, a PTZ units tethered with one formyl group (R-PTZ-CHO) and a CTP subtract contained six terminal amine group (CTP-Hyd) was allowable to endure simple and feasible condensation in ethanol (C_2H_5OH) medium at room temperature by eliminating the water (H_2O) molecules as revealed in **Scheme 1**. Imime (-C=N) bond are typically found in the Schiff's base of hydrazones, however, the hybrid assembly of PTZ on CTP ring described in this chapter.

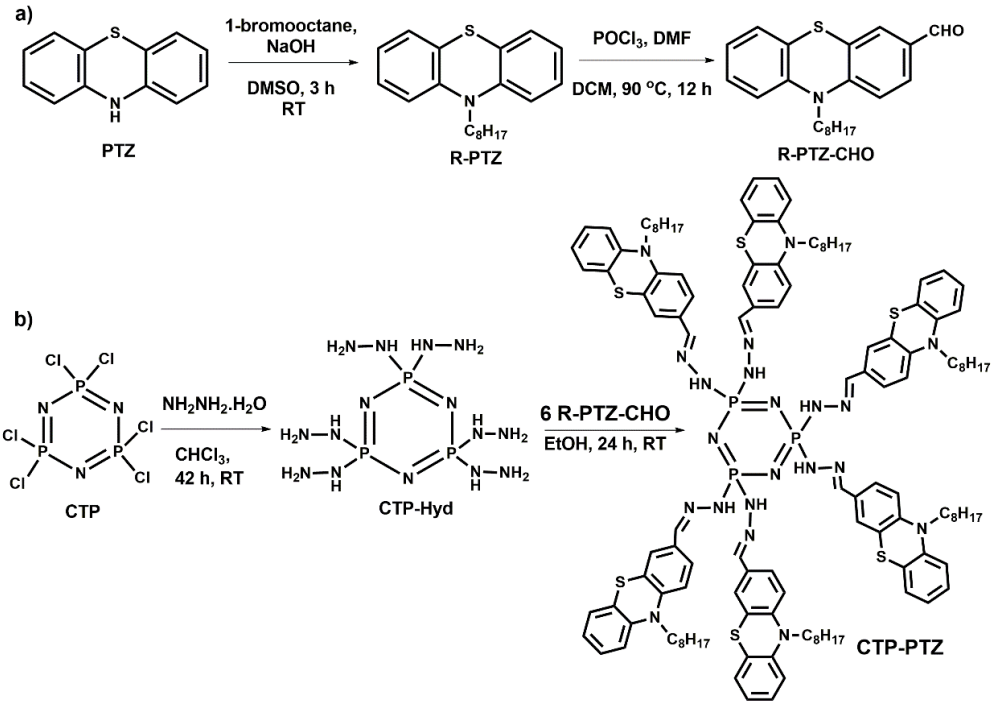

Scheme 1. a) Organic component synthesis for R-PTZ-CHO and b) formation of the final product CTP-PTZ with inorganic component, CTP-Hyd.

III RESULT AND DISCUSSIONS

3.1 ATR-FTIR Data

Both types of significant precursors, CTP-Hyd and R-PTZ-CHO, were synthesised using viable methods, with the outcomes shown in **Figure 1**, and the final hybrid product was described by ATR-FTIR spectroscopy. The information in **Figure 1a** was used to determine the planar structure of the CTP ring. A signal at 1179 cm^{-1} indicated the vibrational frequency of the P-N-P degenerate ring stretching, while 875 cm^{-1} state the frequency of the forbidden symmetric stretching as well as addition signals at 593 and 524 cm^{-1} [39]. As seen in **Figure 1b**, the CTP-Hyd exhibited equivalent signals for N-H stretching at 3332 cm^{-1} and –N-H bending vibration at 1592 cm^{-1} when six terminal primary amines (-NH_2) and integrating secondary amines (-NH-) are linked to the P(V) centre [35]. The presence of the CTP core ring was also confirmed by shifted -P-N stretching vibrational at 1157 cm^{-1}, the vibrational frequency associated with the hydrazide's –N-N bond at 1089 cm^{-1} and a few vibrational frequency appeared between the range of 860 and 520 cm^{-1}. The ART-FTIR data of R-PTZ-CHO as shown in **Figure 1c**, The stretching vibrations of the –CH_3 and –CH_2 groups at 2960 and 2860 cm^{-1} as well as the bending vibrations of the same group at 1460 and 1440 cm^{-1} were used to identify the octyl group (-C_8H_{17}). Additionally, the carbonyl (-C=O) signal for the conjugated aldehyde group (-CHO) was observed at 1685 cm^{-1}, along with the stretching vibrational frequency of –N-CH_2 1465 cm^{-1}, the rocking frequency of long alkyl chains observed at 72 cm^{-1}, and others. The CTP-PTZ assembly produced the spectrum in **Figure 1d**. It can be seen that the signal at 1608 cm^{-1} is the manifestation of the formation of an imine (-C=N-) bond, whereas the signal from the terminal amine group disappears at 3332 and 1592 cm^{-1} [35]. The remaining signals supported the frequencies of the six PTZ units and the P-N framework of the CTP ring core with frequencies at 1470 and 520 cm^{-1} [40].

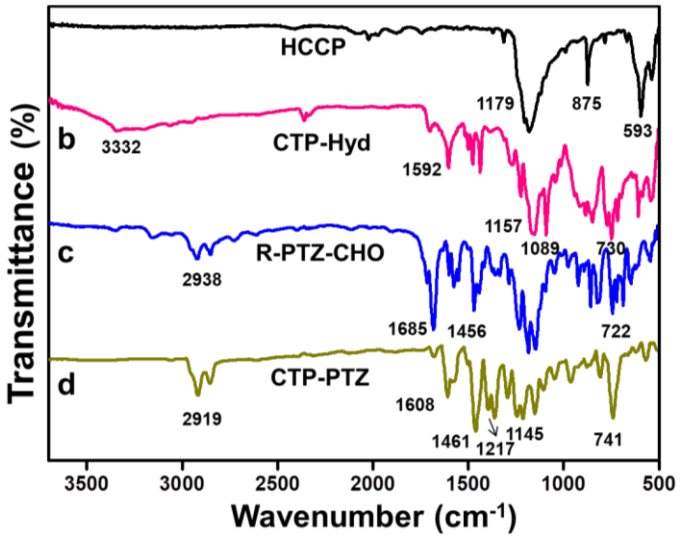

Figure 1. FTIR spectra of a) CTP, b) CTP-Hyd, c) R-PTZ-CHO and d) hybrid molecule, CTP-PTZ

3.2 ^{1}H-NMR data of CTP-PTZ

The ^{1}H-NMR data obtained for CTP-PTZ were used to generate the structure shown in **Figure 2,** which contains six PTZ hydrazone Schiff's base moirties correlated to the CTP ring**.** Since the distinctive aldehyde proton peak of R-PTZ-CHO, this was notice to appear at 9.78 ppm, this peak was disappeared which confirms the formation of CTP-PTZ. The establishment of imine group (-HC=N) was recognized by a sharp singlet peak at 8.52 ppm for six protons (–**H**C=N-) of distinct units. A broad singlet peak notice at 9.79 ppm and the aromatic protons (PTZ) emerged between the range of 6.86 to 7.59 ppm, while the aliphatic protons of the octyl chain (-C_8H_{17}) was found to reveal in the region of 0.88 to 3.87 ppm, which support the six proton in hydrazone (-HC=N-NH-) moieties on CTP core. In contrast to other types of (-HC=N-NH-CO-), where the adjacent electron deficient carbonyl group (C=O) can efficiently deshields to demonstrate a broad peak around between 11.6-11.9 ppm, there was undoubtedly a signal at 9.79 ppm for the hydrazone (-HC=N-N**H**-P) tethered on the P(V) centres of CTP.

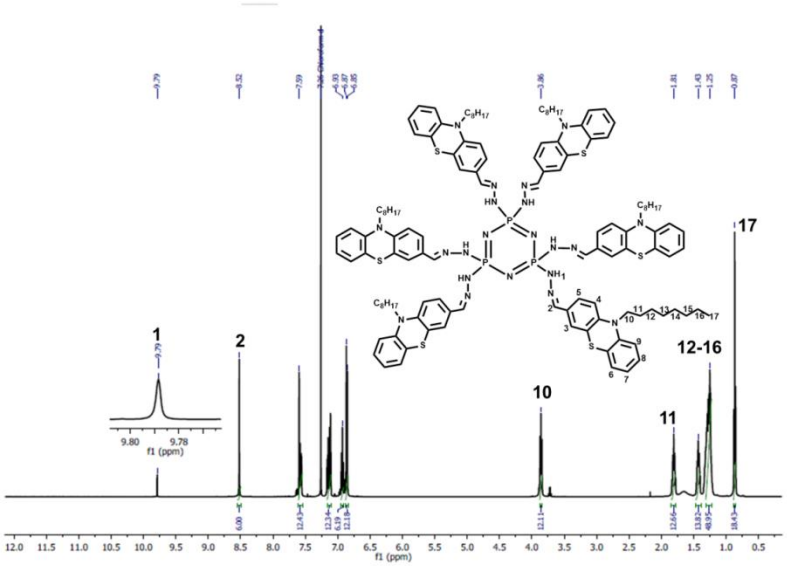

Figure 2. ^{1}H-NMR spectrum of CTP-PTZ

3.3 ^{13}C-NMR data of CTP-PTZ

To additional corroborate the assembly; the ^{13}C-NMR data of CTP-PTZ was collected as depicted in **Figure 3.** All ^{13}C nuclei coincide to the subtract, R-PTZ-CHO only being taken into consideration for the peak assignment in the hybrid inorganic-organic product due to the inorganic core ring has been replaced with six units of hydrazide, rendering only P(V) and nitrogen atoms in the inorganic core. We found to observed at 189.90 ppm in **Figure 2 is** strong ^{13}C-NMR signal for the aldehyde group (-CHO) on the PTZ arm. This signal exhibited a significant upfield region to 160.76 ppm while being converted by condensation into the Schiff base of the imine group (-C=N). In our previous publication on the hydrozone Schiff base Synthesised from hexakis(2-formylphenoxy) cyclophosphazene (HFP-CTP) and salicylic hydrazide (S_{Hyd}), we found to observe that upfield region at 29.14 ppm was higher than the upfield shift at 20.26 ppm [37]. In more details, HFP-CTP was identified to demonstrate a shifted from 188.29 to 167.93 ppm, while the imine bond was generated through condensation with S_{Hyd} [38].

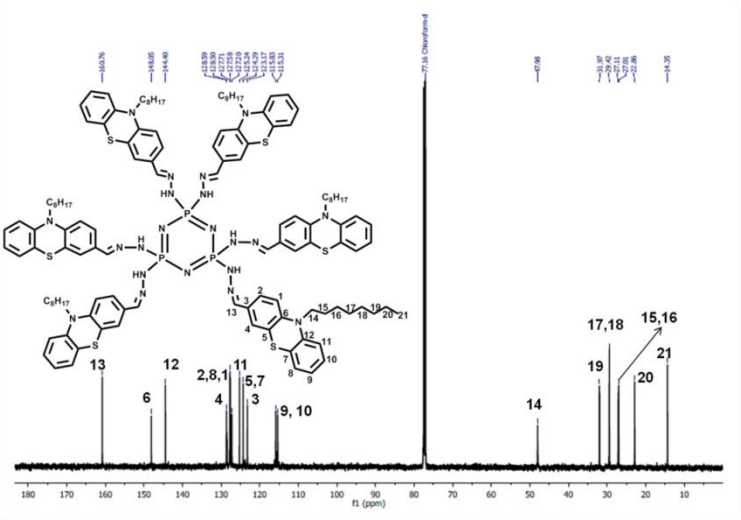

Figure 3. ^{13}C-NMR spectrum of CTP-PTZ

4. Photophysical properties

4.1 Absorption spectra of the precursors and hybrid inorganic-organic compound, CTP-PTZ

The target molecule's photophysical features, such as that tunable absorption, emission band and solvoto-chromism must significantly improve from the initial components to the final product as a critical component in the development of novel multi-chromophoric assembly systems. We conducted steady state photophysical experiments for both the target molecule and the precursors, PTZ, in order to exhibit this property in the multi-component gathering synthesised in the current work. The final inorganic-organic hybrid compound, CTP linked PTZ and the steady state absorbance characteristics of PTZ was studied in the medium of acetonitrile solvent as displayed in **Figure 4**, the absorption spectra of the target compound, CTP-PTZ was associated to that of the precursor PTZ, as well as the significant intermediate molecules R-PTZ and R-PTZ-CHO. In acetonitrile, pristine PTZ notice to appear at 313 nm. The target molecule should be easily soluble in various solvents with divergent polarities and to recognize this objective we have append a long linear alkyl chain (R = $-C_8H_{17}$) to the stiff backbone which achieves the nature of solubilizing group. Although, the alkyl chain has no effect on the PTZ electronic structure, the $-C_8H_{17}$ substituted PTZ (R-PTZ) did not exhibit any noticeable change in the λ_{max} (316 nm). However, as we performed the formylation procedure on R-PTZ to produce R-PTZ-CHO, we notice to observe a significant higher shift in the absorption spectra. The formylated compound exposed two absorption bands: one significantly red shifted band at 386 nm and additional reasonably broad split band nearby 280 and 300 nm. The localised aromatic π-π* transition of the PTZ structure was given higher energy (shorter wavelength) and the charge transfer (CT) transition was given lower energy (longer wavelength). In contrast to the π-π* transition, the CT transition absorption has a lesser intensity. The donor PTZ unit transfers charge to the acceptor aldehyde group, which can be observed in the charge transfer (CT) experiment. Lastly, the absorption spectra of the aimed molecule CTP-PTZ revealed a dramatic bathochromic shift of 25 nm towards higher wavelength, with the peak notice to reveal at 411 nm. PTZ and CTP are covalently attached by an imine linkage, which results in a better electron accepting unit for an enhanced CT mechanism that exhibits a more prominent bathochromic shift than PTZ.

Undoubtedly, the inorganic-organic materials found to observe bathochromic shift towards the visible region. At this point, it is important to note that the basic CTP used as core ring structure displayed a λ_{max} at 175 nm. The aforementioned observations resulted in the following two important conclusions: a) the lengthy liner alkyl chain in the final molecule is soluble in a variety of solvent with relative polarities ranging from 0.099 for toluene to 0.791 for methanol, while the solvent dielectric constants range from 2.38 for toluene and 36.7 for DMF and b) When a multi-chromophoric strategy is used the absorbance spectrum can be adjusted largely.

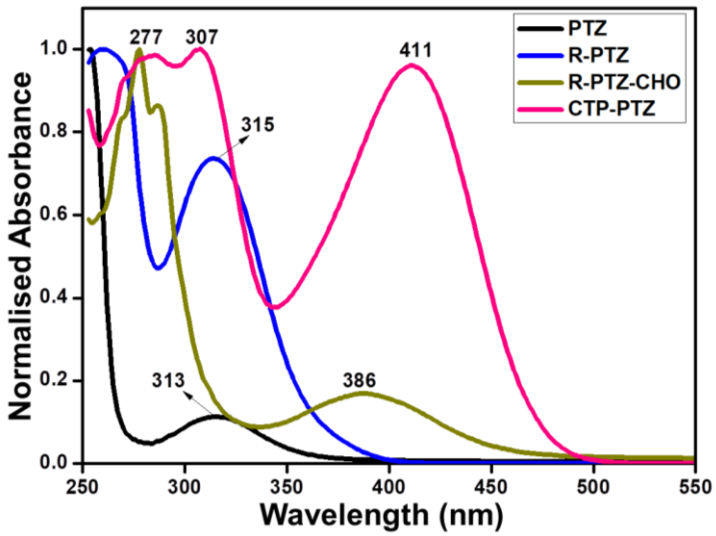

Figure 4. Comparison UV-Vis spectra of PTZ, R-PTZ, R-PTZ-CHO and hybrid inorganic-organic molecule, CTP-PTZ

4.2 Studies of steady state absorption in different solvent

As illustrated in **Figure 5**, UV-Vis absorption spectra of CTP-PTZ were recorded in a variety of solvents at room temperature (25 ^{o}C). Two absorption bands (λ_{max}), one near 300 nm and the second peak reported to be noticeable during bathochromic shift at 410-420 nm depending on the solvent. The hybrid compound, CTP-PTZ demonstrated a molar absorptivity (ε) that was relatively high (10^4 M^{-1} cm^{-1}) in entirely the solvents that were being investigated. The profile and curved of the absorption spectra are not at all conveyed by any of the solvent. As we change from a non-polar solvent (toluene, 411 nm) to polar solvent (n-butanol, 416 nm), we found to reveal a very little bathochromic shift in the λ_{max} of the charge transition state. The slightly positive solvatochromism that was observed indicates an inorganic-organic hybrid molecule was synthesised in a polar protic solvent environment, while results in slight variations in the ground state dipole moments [32].

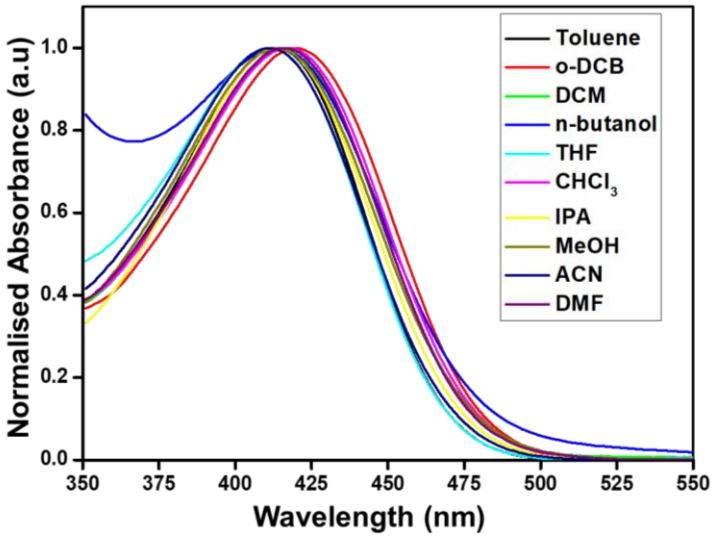

Figure 5. Comparison of CTP-PTZ absorption spectra (CT band) measured in various solvent and normalised. Inset: CTP-PTZ absorption data in various solvents.

4.3 Studies of steady state emission in different solvent

After establishing the ground state features of the synthesised CTP-PTZ compound, we moved on to determining the excited state behaviour. For the emission investigation, we excited the molecule at the proper peak (CT state), and we evaluated the emission data using different solvents as shown in **Figure 6**. **In Table 1**, we summarise the photophysical data used in the investigation, such as the maximum values (λ_{max}) of the absorption and emission spectra, as well as the dielectric constant and refractive index values of the solvents used. When related to the λ_{max}, the hybrid molecule's emission data displayed remarkable behaviours. In all of the different solvent employed in this experiment, the measured emission spectra exhibited a λ_{max} between 515 to 597 nm, which was an adequately broad spectrum. The measured emission maxima obviously endured a significant bathochromic shift with an increase in solvent polarity, demonstrating the CT nature of the electronic transition. It's fascinating to observe that, rather than the molecules ground state, the solvent has a more dramatic impact on the excited state of the molecule. This is perfectly associated with the measured emission maxima in toluene, which was 515 nm and moves to 541 nm, when we slightly raise the solvent polarity and change to solvents like, chloroform ($CHCl_3$) and methylene chloride (CH_2Cl_2, DCM). When we moved to polar-aprotic solvent like acetonitrile (CH_3CN), where the emission spectrum was noticed at 583 nm, an even higher bathochromic shift we observed. Polar protic solvents like methanol (597 nm) showed revealed further shifts towards longer wavelengths. The observed significant bathochromic change in the emission maxima when we switched form a non-polar to a polar solvent demonstrate that the excited state is stabilised in polar solvents, or to express it another way, the excited state dipole moment is larger than that of the ground state. The excited state energy level is decreased a as result of this interaction, which increases the rate of non-radiative deterioration. Similar activity was previously reported with a variety of different compounds, which is the stabilising of the molecular excited state in polar medium with lower energy level and consequently emitting at longer wavelengths [41-42].

Additionally, the emission profile reveals two other noteworthy characteristic: first, the emission band full width at half maximum (FWHM) increases with solvent polarity or when changing from toluene to methanol and second, the synthesised CTP-PTZ emits more strongly in non-polar solvents than in polar protic solvents, which is consistent with the nature of a charge transfer state. The following observations are made as we conclude up this part. With the observed bathochromic shift of 82 nm, it is possible to determine that there is (i) tunable emission from the yellow to green region depending on the solvent used, (ii) higher positive solvatochromism with increasing solvent polarity, and (iii) self quenching effect is minimised due to excitation and emission wavelength are more distant form one another.

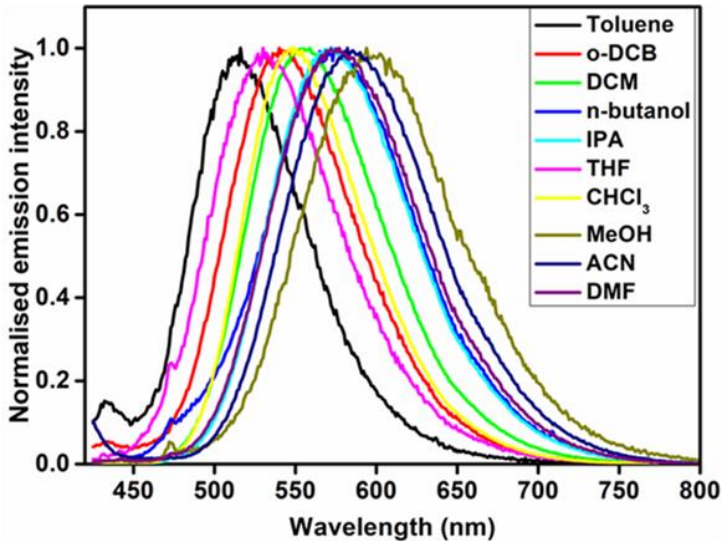

Figure 6. Comparison of CTP-PTZ emission spectra (CT band) measured in various solvent and normalised. Inset: CTP-PTZ absorption data in various solvents.

4.4 Polarizability of Stokes shift and solvent orientation

The solvent behaviour, as we noticed in the preceding section (4.2 and 4.3), is essential for the spectroscopy features that are detected. In an effort to gain an detailed understanding this incidence, we tried to associate two parameters. i) Solvent orientation polarizabilty (Δf), which depends on the solvent's refractive index (n) and dielectric constant (ε), solely accounts for the spectrum shifts resulting by the reorientation of the solvent behaviours [43,44], and ii) Stokes shift, which is a distinction between the maximum emission and absorption wavelengths [45]. We plotted the CTP-PTZ emission maxima in each solvent against the equivalent solvent's dielectric constant value because this parameter frequently denotes solvent polarity. This demonstrated how the solvent's polarity affects the excited state in a substantial way. Considering the emission peak maxima, a suitably sufficient linear trend (R_2 = 0.78 was detected), with the maximum shifting from 515 nm to 597 nm with rising solvent dielectric constant as depicted in **Figure 7**.The fact that the emission maxima are not directly correlated with the solvent's dielectric characteristics is typical of the weak interaction between solvents and chromophores. After understanding more about the effects of the dielectric constant on the excited state, we calculated the Stokes shift for CTP-PTZ in various solvents, and the results are displayed in **Table 1**. In the Stokes shift values between the ranges of 4796 to 7463 cm^{-1}. The fact that the charge distribution is diverse in the excited state as related to the ground state essentially allows the Stokes shift values to significantly increases with an increase in solvent polarity, as demonstrated in the **Table 1**. It was attempted to plot the measured Stokes shift (υ) against the solvent polarity parameter Δf (ε, n), which is known as the Lippert-Mataga plot and takes into consideration the general solvent impact [46,47]. In **Figure 7,** the slope's magnitude can be used to estimate the difference between the excited state and ground state dipole moment. The expression for Δf (ε, n) is as follows

$$\Delta f\ (\varepsilon) = [(\varepsilon - 1)/(2\varepsilon + 1)] - [(n^2 - 1)/(2n^2 + 1)]$$

Table 1. CTP-PTZ photophysical data measured in a variety of solvents.

Solvent	Refractive index	Dielectric constant	Relative polarity	Absorption maxima (λ_{abs}, nm)	υ_{abs} (cm^{-1})	Emission maxima (λ_{ems}, nm)	υ_{ems} (cm^{-1})	υ_{abs} (cm^{-1}) - υ_{ems} (cm^{-1})	Δf
Toluene	1.4961	2.38	0.099	413	24213	515	19417	4796	0.013
THF	1.4050	7.52	0.207	413	24213	529	18904	5309	0.210
$CHCl_3$	1.4459	4.81	0.259	420	23809	541	18484	5325	0.150
DCM	1.4244	8.93	0.309	419	23866	555	18018	5848	0.217
ODCB	1.5515	9.93	-	420	23810	539	18553	5257	0.186
DMF	1.4305	36.70	0.386	416	24038	574	17422	6616	0.274
ACN	1.3442	36.64	0.786	411	24331	583	17153	7178	0.305
IPA	1.3776	20.18	0.546	414	24155	572	17483	6672	0.277
BuOH	1.3988	17.50	0.586	415	24096	569	17575	6521	0.264
MeOH	1.3288	32.70	0.791	413	24213	597	16750	7463	0.308

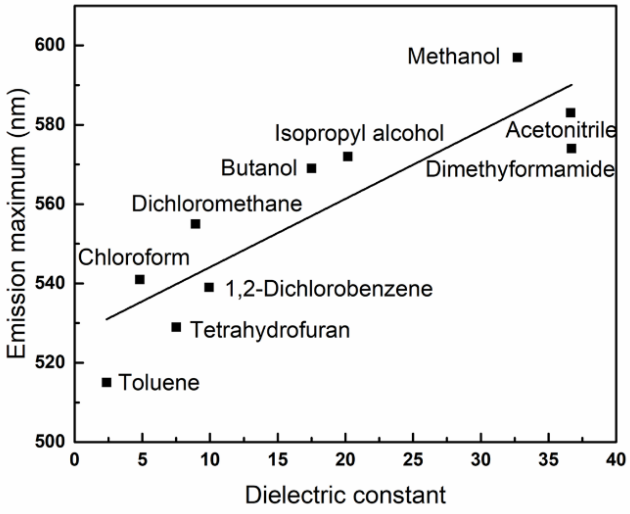

Figure 7. Plot of solvent dielectric constant vs emission maximum

In Figure 8a, illustrates a weak but adequate linear relationship between the polarity of the solvent and the magnitude of the stoke shift. Two significant results could be obtained from this plot: i) when the Δf value exceeds 0.22, the majority of the data points fall along a straight line, and ii) solvents that did not follow the trend, possessed polarity values lower than 0.03. The linear correlation fit significantly improved with an R_2 value standing at 0.91 once this specific non-polar solvent (toluene) was removed as revealed in **Figure 8b**. These results suggest that the Stokes shift may be affected by additional solvent effects, such as H-bonding, in addition to polarity [47]. This assertion can be emphasised by using the plot's polar solvent region. According to **Figure 8b**, the hybrid molecule Stokes shift in methanol was a little higher than what the linear trend line was indicated. This could be the hydrazine unit of CTP-PTZ and the –OH group in methanol produced a hydrogen bond, which causing the observed Stoke shift and an H-bonding substance, it is challenging to determine the comparative magnitudes of polarization and H-bonding interactions. According to the plots of positive slope for CTP-PTZ compound, the excited dipole moments improve greater as the polarity increases.

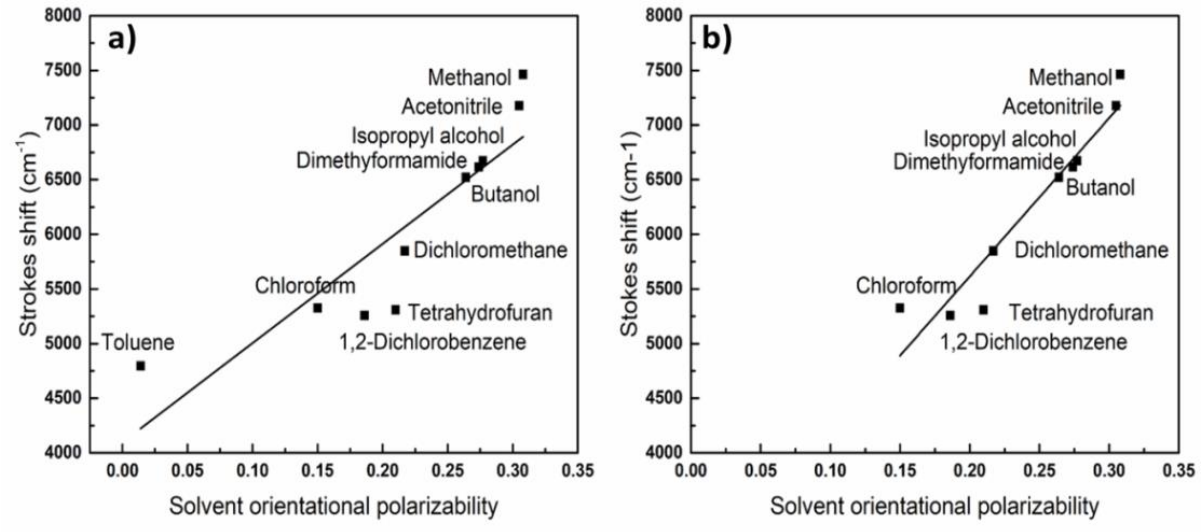

Figure 8. Lippert-mataga a) Stokes shift in wavenumbers vs. solvent orientation polarizability, Δf (ε, n) and b) Stokes shift in wavenumber vs. solvent orientation polarizability (excluded toluene)

5. Cyclic voltammetry analysis (CV)

5.1 Cyclic voltammetry analysis of the precursor and hybrid material, CTP-PTZ

We encouraged to identifying the energy levels of the synthesised hybrid material through the extensive photophysical behaviours described the previous section. Since the energy of the HOMO corresponds to the onset oxidation potential, CV data was examined to demonstrate the molecule HOMO levels. Since the HOMO level, $E_{0\text{-}0}$ value and the LUMO energy level subsequently calculated. CV data of CTP-PTZ was collected in the medium of acetonitrile (CH_3CN) under nitrogen environment as depicted in **Figure 9**. The oxidation onset potential value (using Ferrocene (Fc/Fc^+) as an internal standard) reveals an E_{HOMO} value of -4.93 eV. Using the formula of E_{LUMO}= E_{HOMO}-$E_{0\text{-}0}$, we have determined the LUMO level, E_{LUMO}. The junction places of the normalized absorption and emission profile was used to estimate the $E_{0\text{-}0}$ transition energy. Since, no entropy change occurred during the light excitation, the estimated E_{LUMO} value was found to be -2.25 eV. More study is currently being done in this area since the material's energy level value employed as a charge transfer (CT) material in hybrid pervovskite solar cells.

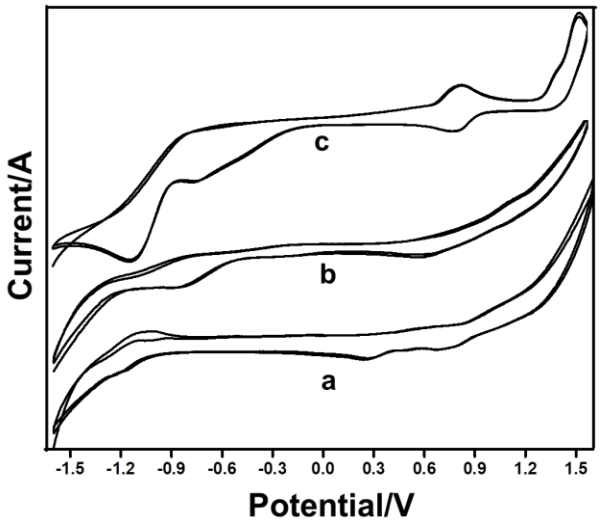

Figure 9. CV curve of the precursors, a) PTZ, b) CTP, and c) redox performance of hybrid molecule, CTP-PTZ

5.2 Variant of scan rates

The supportive electrolyte, Bu_4NPF_6 solution (0.1 M), was utilised during the recording of the CV data in acetonitrile medium under N_2 atmosphere at different scan rates, such as that 10, 25, 50, 75 and 100 mV/s. The anodic and cathodic peaks on the CV are clearly visible as displayed in **Figure 10a**. It was found that CTP-PTZ one electron transfer redox mechanism is nearly irreversible. Pristine CTP and PTZ collected under the identical condition which did not exhibit any distinct redox peaks on a cyclic voltammogram (**Figure 10**). This result demonstrates that the homogenous assembly of PTZ units via Schiff base motifs by condensation on the periphery of CTP core has in fact a significant impact on the redox behaviours. The peak current intensity, increases proportionately with respect to the increases in scan rates as observed in cyclic voltammogram analysis at several scan rates such as 10, 25, 50, 75 and 100 mV/s). In contrast, it was stated that the redox potential measurement exhibited negligible change with different scan rates. Additionally, it was determined that the peak observed form of all CV data consistently displayed a single type of redox activity at all scan rates. All six of the PTZ units on the CTP core was found to executed redox processes simultaneously, as proven by the single redox potential and we previously reported on similar type of redox performance on a multi-ferrocene assembly on CTP core.

In Addition, the electrochemical progression taking place at the electrode edge. In order to understand the process occurring at electrode we have plotted the variation of current intensity (both anodic and cathodic) against the square root of scan rates between the 10 to 100 mV/s. An excellent least squares relationship found to reveal for the oxidation (R_2 = 0.997) and reduction (R_2 = 0.977) processes as depicted in **Figure 10b**.

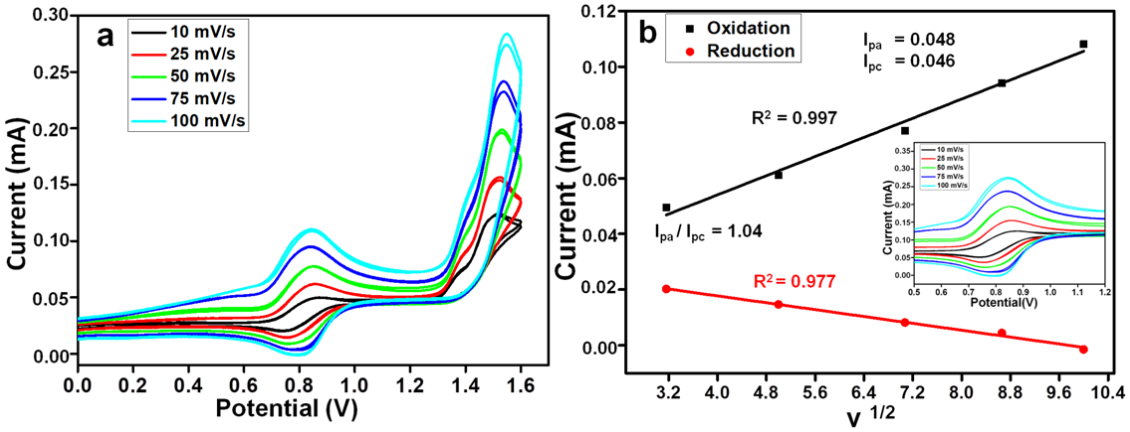

Figure 10. Comparison CV profile of a) hybrid molecule, CTP-PTZ examined at several scan rates and b) linear correlation plot for the square root of anodic and cathodic current vs scan rates.

6. TGA data

Our intention was to explore the inorganic-organic hybrid molecule's thermal stability in addition to its robust characteristic and prospective photo stability. The primary parameter typically used to determine thermal stability is the onset degradation temperature (T_d). To ascertain the thermal properties of the material being analysed, such as R-PRZ-CHO, CTP-Hyd and hybrid molecule, CTP-PTZ, TGA curve was examined under inert condition form room temperature to 1000 ^oC as revealed in **Figure 11**. The Thermal degradation (T_d) values of R-PTZ-CHO, CTP-Hyd and CTP-PTZ notice to observed at 153 ^oC, 280 ^oC and 326 ^oC respectively. The data for the hybrid compound, CTP-PTZ demonstrated outstanding thermal behaviour due to the presence of a flame-retardant characteristic resulting from the P-N structure in the CTP core [49-51]. The initial mass losses at 100 ^oC which is due to existence of moisture present in the material being analysed. The decomposition of the structure's skeleton and existing functional group was represented by the TGA profile's many degradation phase in the curve. The minimal residual mass (3.1 %) found to notice for the pure organic composition of R-PTZ-CHO. In the CTP-Hyd revealed the highest amount of residual mass (37.6 %) due to the significant proportion of P-N frameworks with hydrazide arms relative to inorganic core. As a hybrid molecule, CTP-PTZ exhibited the enrichment in thermal stable behaviour with high value of T_d (326 ^oC) and the substantial quantity of residual mass (34.8 %) due to the presence of P-N heterocycle in the CTP core ring structure.

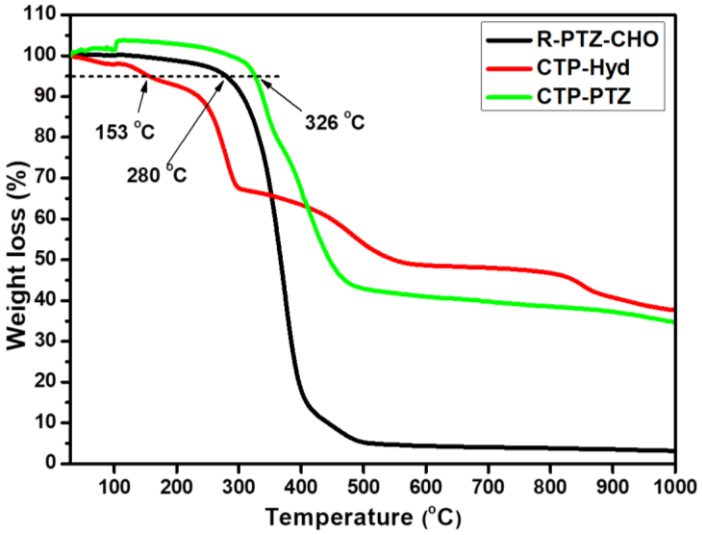

Figure 11. TGA curves of R-PTZ-CHO, CTP-Hyd and hybrid molecule, CTP-PTZ

CONCLUSION

The formation of the hybrid luminous material, CTP-PTZ, which consist six units of PTZ Schiff bases designed on the periphery of inorganic core known as CTP, has been described for the first time. By using ATR-FTIR, ^{1}H-NMR and ^{13}C-NMR data the structure of the synthesised molecules was conclusively confirmed. As a result of the multicomponent structure of organic chromophores on the stable inorganic core, intriguing photophysical, electrochemical as well as thermal features was examined. Particularly**,** it was found that the positive solvatochromism properties increased with solvent polarity, and that the emission from yellow to green region was observed. The presence of the P-N structure in CTP core, contributes flame retardant behaviour to the hybrid molecule of CTP-PTZ which found to observed excellent thermal stability at 326 ^{o}C.

ACKNOWLEDGMENT

All Figures taken with permission from the Royal Society of Chemistry, a reproduced of Ref. [32] has been made.

ABBREVIATION

HCCP	Hexachlrocyclotriphosphazne
CTP	Cyclophosphazne
CTP-Hyd	Cyclophosphazene hydrazide
CT	Charge transfer
R-PTZ-CHO	10-octly-10H-phenothiazine-3-carbaldehyde
PTZ	Phenothiazine
$POCl_3$	Phosphorus oxychloride
ATR-FTIR	Attenuated total reflectance Fourier transforms infrared spectroscopy
^{1}H-NMR	Proton nuclear magnetic resonance
^{13}C-NMR	Carbon-13 nuclear magnetic resonance
CV	cyclic voltammeter
TGA	Thermo gravimetric analysis
DMF	N-N'-dimethylformamide
HOMO	Highest occupied molecular orbital
LUMO	Lowest unoccupied molecular level
Bu_4NPF_6	Tetrabutylammonium hexafluorophosphate

REFERENCES

[1] Lebeau, B. and Innocenzi, P., Hybrid materials for optics and photonics. *Chemical Society Reviews*, 2011, *40*, 886-906.

[2] Astruc, D., Boisselier, E. and Ornelas, C., Dendrimers designed for functions: from physical, photophysical, and supramolecular properties to applications in sensing, catalysis, molecular electronics, photonics, and nanomedicine. *Chemical reviews*, *110*, 1857-1959.

[3] Ashford, D.L., Gish, M.K., Vannucci, A.K., Brennaman, M.K., Templeton, J.L., Papanikolas, J.M. and Meyer, T.J., 2015. Molecular chromophore–catalyst assemblies for solar fuel applications. *Chemical Reviews*, *115*(23), pp.13006-13049.

[4] Wang, J.C., Hill, S.P., Dilbeck, T., Ogunsolu, O.O., Banerjee, T. and Hanson, K., Multimolecular assemblies on high surface area metal oxides and their role in interfacial energy and electron transfer. *Chemical Society Reviews*, 2018, *47*, 104-148.

[5] Brauge, L., Veriot, G., Franc, G., Deloncle, R., Caminade, A.M. and Majoral, J.P., 2006. Synthesis of phosphorus dendrimers bearing chromophoric end groups: toward organic blue light-emitting diodes. *Tetrahedron*, *62*(51), pp.11891-11899.

[6] Chetan, B., and Chain-Shu, H., Organic Nanoparticles and Organic-Inorganic Hybrid Nanocomposites: Synthesis and Photophysical Characterization, Lambert Academic Publishing, 2011.

[7] Mahmud, A., Khan, A.A., Islam, S., Voss, P. and Ban, D., Integration of organic/inorganic nanostructured materials in a hybrid nanogenerator enables efficacious energy harvesting via mutual performance enhancement. *Nano Energy*, 2019, *58*, 112-120.

[8] Sanchez, C., Belleville, P., Popall, M. and Nicole, L., Applications of advanced hybrid organic–inorganic nanomaterials: from laboratory to market. *Chemical Society Reviews*, *40*, 2011, 696-753.

[9] Hassan, Z., Matt, Y., Begum, S., Tsotsalas, M. and Bräse, S., Assembly of Molecular Building Blocks into Integrated Complex Functional Molecular Systems: Structuring Matter Made to Order. *Advanced Functional Materials*, 2020, p.1907625.

[10] Lees, A. J. ed., *Photophysics of organometallics* 2010, Vol. 29, Springer Science & Business Media.

[11] Wei, Y., Laurent, R., Majoral, J.P. and Caminade, A.M., Synthesis and characterization of phosphorus-containing dendrimers bearing rhodamine derivatives as terminal groups. *Arkivoc*, 2010, *10*, 318-327.

[12] Qiu, J., Hameau, A., Shi, X., Mignani, S., Majoral, J.P. and Caminade, A.M., Fluorescent Phosphorus Dendrimers: Towards Material and Biological Applications. *ChemPlusChem*, 2019, *84*, 1070-1080.

[13] 20. Xue, P., Yao, B., Liu, X., Sun, J., Gong, P., Zhang, Z., Qian, C., Zhang, Y. and Lu, R., Reversible mechanochromic luminescence of phenothiazine-based 10, 10′-bianthracene derivatives with different lengths of alkyl chains. *Journal of Materials Chemistry C*, 2015, *3*, 1018-1025.

[14] Brauge, L., Caminade, A.M., Majoral, J.P., Slomkowski, S. and Wolszczak, M., Segmental mobility in phosphorus-containing dendrimers, Studies by fluorescent spectroscopy. *Macromolecules*, 2001, *34*, 5599-5606.

[15] Jia, J. and Wu, Y., Alkyl length dependent reversible mechanofluorochromism of phenothiazine derivatives functionalized with formyl group. *Dyes and Pigments*, 2017, *147*, 537-543.

[16] Sachdeva, T., Bishnoi, S. and Milton, M.D., Multi-Stimuli Response Displaying Novel Phenothiazine-Based Non-Planar D-π-A Hydrazones: Synthesis, Characterization, Photophysical and Thermal studies. 2017, *ChemistrySelect*, *2*, 11307-11313.

[17] Gai, F., Li, X., Zhou, T., Zhao, X., Lu, D., Liu, Y. and Huo, Q., Silica cross-linked nanoparticles encapsulating a phenothiazine-derived Schiff base for selective detection of Fe (III) in aqueous media. *Journal of Materials Chemistry B*, 2014, *2*, 6306-6312.

[18] Chandrasekhar, V., Azhakar, R., Murugesapandian, B., Senapati, T., Bag, P., Pandey, M.D., Maurya, S.K. and Goswami, D., Synthesis, Structure, and Two-Photon Absorption Studies of a Phosphorus-Based Tris Hydrazone Ligand (S) P [N (Me) N-CH-C_6H_3-2-OH-4-N $(CH_2CH_3)_2]_3$ and Its Metal Complexes. *Inorganic chemistry*, 2010, *49*, 4008-4016.

[19] Chandrasekhar, V. and Thomas, K.J., Coordination and organometallic chemistry of cyclophosphazenes and polyphosphazenes. *Applied organometallic chemistry*, 1993, *7*, 1-31.

[20] Chandrasekhar, V. and Nagendran, S., Phosphazenes as scaffolds for the construction of multi-site coordination ligands. *Chemical Society Reviews*, 2001, *30*, 193-203.

[21] V. Chandrasekhar, *Inorganic and Organometallic Polymers*, Springer-Verlag, 2005.

[22] Mukundam, V., Dhanunjayarao, K., Mamidala, R. and Venkatasubbaiah, K., Synthesis, characterization and aggregation induced enhanced emission properties of tetraaryl pyrazole decorated cyclophosphazenes. *Journal of Materials Chemistry C*, 2016, *4*, 3523-3530.

[23] İbişoğlu, H., Kılıç, Z., Yuksel, F. and Tümay, S.O., 2020. Synthesis, characterization, photophysical and intramolecular energy transfer properties of oxy-naphthylchalcone appended cyclotriphosphazene cores. *Journal of Luminescence*, *222*, p.117125.

[24] Rao, M.R., Bolligarla, R., Butcher, R.J. and Ravikanth, M., Hexa boron-dipyrromethene cyclotriphosphazenes: synthesis, crystal structure, and photophysical properties. *Inorganic chemistry*, 2010, *49*, 10606-10616.

[25] Nair, V.S., Pareek, Y., Karunakaran, V., Ravikanth, M. and Ajayaghosh, A., Cyclotriphosphazene appended porphyrins and fulleropyrrolidine complexes as supramolecular multiple photosynthetic reaction centers: Steady and excited states photophysical investigation. *Physical Chemistry Chemical Physics*, 2014, *16*, 10149-10156.

[26] Ün, İ., İbişoğlu, H., Ün, Ş.Ş., Çoşut, B. and Kılıç, A., Syntheses, characterizations, thermal and photophysical properties of cyclophosphazenes containing adamantane units. *Inorganica Chimica Acta*, 2013, *399*, 219-226.

[27] Uslu, A., Tümay, S.O., Şenocak, A., Yuksel, F., Özcan, E. and Yeşilot, S., Imidazole/benzimidazole-modified cyclotriphosphazenes as highly selective fluorescent probes for Cu^{2+}: synthesis, configurational isomers, and crystal structures. *Dalton Transactions*, 2017, *46*, 9140-9156.

[28] Özcan, E., Tümay, S.O., Alidağı, H.A., Çoşut, B. and Yeşilot, S., A new cyclotriphosphazene appended phenanthroline derivative as a highly selective and sensitive OFF–ON fluorescent chemosensor for Al^{3+} ions. *Dyes and Pigments*, 2016, *132*, 230-236.

[29] Haddon, R.C., Mayo, S.L., Chichester, S.V. and Marshall, J.H., Phenalene-phosphazene complexes: injection of electron spin density into the cyclotriphosphazene ring system. *Journal of the American Chemical Society*, 1985, *107*, 7585-7591.

[30] Haddon, R.C., Chichester-Hicks, S.V. and Mayo, S.L., Phenalene-phosphazene complexes: effect of exocyclic charge densities on the cyclotriphosphazene ring system. *Inorganic Chemistry*, 1988, *27*, 1911-1915.

[31] Çiftçi, G.Y., Şenkuytu, E., Durmuş, M., Yuksel, F. and Kılıç, A., Structural and fluorescence properties of 2-naphthylamine substituted cyclotriphosphazenes. *Inorganica Chimica Acta*, 2014, *423*, 489-495.

[32] Chelike, D.K., Alagumalai, A., Muthukumar, V.R., Thangavelu, S.A.G. and Krishnamoorthy, A., 2020. Tunable yellow–green emitting cyclotriphosphazene appended phenothiazine hydrazone hybrid material: Synthesis, characterisation, photophysical and electrochemical studies. *New Journal of Chemistry*, 44(31),13401-13414.

[33] Majoral, J.P. and Caminade, A.M., 2019. Phosphorhydrazones as Useful Building Blocks for Special Architectures: Macrocycles and Dendrimers. *European Journal of Inorganic Chemistry*, *2019*(11-12), pp.1457-1475.
[34] Galliot, C., Caminade, A.M., Dahan, F. and Majoral, J.P., Synthesis, Structure, and Reactivity of Stable PN Heterocycles with Two and Six Methyleneamine Units: $[H_2C=N=N(Me)]_2P(S)(Ph)$ and $[H_2C=N=N(Me)]_6P_3N_3$. *Angewandte Chemie International Edition*, 1993, *32*, 1477-1479.
[35] Chandrasekhar, V., Senthil A. Gurusamy Thangavelu, Nagendran, S., Krishnan, V., Azhakar, R., Butcher, R. J. Cyclophosphanzene hydrazides as scaffolds for multi-ferrocenyl assemblies: Synthesis, structures and electrochemistry *Organometallics***,** 2003, *22*, 976 – 986
[36] Chandrasekhar, V., Senthil A. Gurusamy Thangavelu, Azhakar, R., Pandian, B. M. Cyclophosphazene-supported tetranuclear copper assembly containing fifteen contiguous inorganic rings. *Inorg. Chem.* 2008, *47*, 1922-1924
[37] Chandrasekhar, V., Senthil A. Gurusamy Thangavelu, Azhakar, R., Pandian, M. 36- and 42- Membered cyclophosphazene-containing macrocycles *Tetrahedron Lett.*, 2006**,** *47*, 8365-8368.
[38] Dinesh Kumar, C., Ananthan Alagumalai, Joydev Acharya, Pawan Kumar, Koustav Sarkar, Senthil A. Gurusamy Thangavelu, Vadapalli Chandrasekhar. "Functionalized Iron Oxide Nanoparticles Conjugate of Multi-Anchored Schiff's Base Inorganic Heterocyclic Pendant Groups: Cytotoxicity Studies." *Applied Surface Science*, 2020, *501*, 143963.
[39] Çiftçi, G.Y., Şenkuytu, E., Durmuş, M., Yuksel, F. and Kılıç, A. Structural and fluorescence properties of 2-naphthylamine substituted cyclotriphosphazenes. Inorganica Chimica Acta, ., 2014, 423, pp.489-495.
[40] Majoral, J.P. and Caminade, A.M. Phosphorhydrazones as useful building blocks for special architectures: macrocycles and dendrimers. European Journal of Inorganic Chemistry, 2019 (11-12), pp.1457-1475.
[41] Galliot, C., Caminade, A.M., Dahan, F. and Majoral, J.P. Synthesis, Structure, and Reactivity of Stable PN Heterocycles with Two and Six Methyleneamine Units:$[H_2C=N-N(Me)]_2P(S)(Ph)$ and $[H_2C=N-N(Me)]_6P_3N_3$. Angewandte Chemie International Edition in English, 1993, 32(10), pp.1477-1479.
[42] Chandrasekhar, V., Senthil Andavan, G.T., Nagendran, S., Krishnan, V., Azhakar, R. and Butcher, R.J.. Cyclophosphazene hydrazides as scaffolds for multi-ferrocenyl assemblies: synthesis, structure, and electrochemistry. Organometallics, 2003, 22(5), pp.976-986.
[43] Chandrasekhar, V., Andavan, G.T.S., Azhakar, R. and Pandian, B.M. Cyclophosphazene-supported tetranuclear copper assembly containing 15 contiguous inorganic rings. Inorganic chemistry, 2008, 47(6), pp.1922-1924.
[44] Chandrasekhar, V., Andavan, G.T.S., Azhakar, R. and Pandian, B.M. 36-and 42-Membered cyclophosphazene-containing macrocycles. Tetrahedron letters, 2006, 47(47), pp.8365-8368.
[45] Xie, Z., Midya, A., Loh, K.P., Adams, S., Blackwood, D.J., Wang, J., Zhang, X. and Chen, Z., Highly efficient dye-sensitized solar cells using phenothiazine derivative organic dyes. Progress in Photovoltaics: Research and Applications, 2010, 18(8), pp.573-581.
[46] Allcock, H.R. Recent advances in phosphazene (phosphonitrilic) chemistry. chemical Reviews, 1972, 72(4), pp.315-356.
[47] Dey, J. and Warner, I.M. Charge-transfer effects on the fluorescence spectra of 9-aminocamptothecin steady-state and time-resolved fluorescence studies. Journal of Photochemistry and Photobiology A: Chemistry, 1998, 116(1), pp.27-37.
[48] Vázquez, M.E., Blanco, J.B. and Imperiali, B. Photophysics and biological applications of the environment-sensitive fluorophore 6-N, N-dimethylamino-2, 3-naphthalimide. Journal of the American Chemical Society, 2005, 127(4), pp.1300-1306.
[49] Lakowicz, J.R. ed.. Principles of fluorescence spectroscopy. Boston, MA: springer US 2006.
[50] Srividya, N., Ramamurthy, P. and Ramakrishnan, V.T. Solvent effects on the absorption and fluorescence spectra of some acridinedione dyes: determination of ground and excited state dipole moments. Spectrochimica Acta Part A: Molecular and Biomolecular Spectroscopy, 1997, 53(11), pp.1743-1753.
[51] Chelike, D.K., Alagumalai, A., Muthukumar, V.R., Thangavelu, S.A.G. and Krishnamoorthy, A.,. Tunable yellow–green emitting cyclotriphosphazene appended phenothiazine hydrazone hybrid material: Synthesis, characterisation, photophysical and electrochemical studies. New Journal of Chemistry, 2020, 44(31), pp.13401-13414.